

Screening of Possible Re-Substitutional Elements in Single-Crystal Ni-Based Superalloys: A Viewpoint From Interdiffusion Coefficients in Ni-Al-X Ternaries



JUAN CHEN, LIJUN ZHANG, and XIAO-GANG LU

A popular area of research in the field of high-temperature alloys concerns the search of substitutional elements for Re in order to manufacture single-crystal Ni-based superalloys with less or even no Re addition. To find the elements with similar or even lower diffusion coefficients than Re is an effective strategy. Based on 29 fcc diffusion couples in ternary Ni-Al-X ($X = \text{Re, Os, and Ir}$) systems, high-throughput measurement of composition- and temperature-dependent interdiffusivity matrices was performed using our recently developed numerical inverse method implemented in HitDIC software. The reliability of the determined interdiffusivities was validated by comprehensively comparing the model-predicted composition/interdiffusion flux profiles for each diffusion couple with the corresponding experimental data. Moreover, we also conducted a comparison with the interdiffusivities evaluated using the traditional Matano–Kirkaldy method as well as those from the literature and in boundary binary systems. After that, a comprehensive comparison of the interdiffusion coefficients in fcc Ni-2 wt pct Al-6 wt pct X ($X = \text{Ti, Co, Ni, Nb, Mo, Ru, Rh, Ta, W, Re, Os, Ir, and Pt}$) alloys at 1423 K to 1573 K was conducted. Results indicate that the diffusion rate of Re is lower than that of Os at 1473 K and 1523 K; but higher at 1573 K, while the diffusion rate of Ir is always slightly higher than those of Os and Re at 1473 K to 1573 K. Further analysis of the magnitude of the interdiffusion coefficient correlates with the alloying concentration, activation energy, atomic number, and atomic radius of different diffusing transition metal species (*i.e.*, Ti, Co, Ni, Nb, Mo, Ru, Rh, Ta, W, Re, Os, Ir, and Pt) was conducted, which is expected to provide useful information regarding element choice in the development of new-generation Ni-based single-crystal superalloys.

<https://doi.org/10.1007/s11661-018-4669-1>

© The Minerals, Metals & Materials Society and ASM International 2018

I. INTRODUCTION

GIVEN their superior high-temperature mechanical and physical properties, single-crystal (SX) Ni-based superalloys are widely applied as the main high-temperature parts in aero-engine and turbine blades.^[1,2] However, in order to meet the increasing inlet temperature requirements of aero-engine turbines, the high-temperature properties of SX Ni-based superalloys must be further improved. SX Ni-based superalloys have been

developed from the 1st to 6th generation in the past few decades and will continue to evolve in the future. Creep is one of the key factors in controlling the lifetimes of SX Ni-based superalloys at elevated service temperatures. An effective strategy to increase lifetime is to improve creep resistance. As proposed by Reed,^[3] in the steady-state regime, for pure nickel the creep strain rate $\dot{\epsilon}$ and the diffusion coefficient D of pure nickel are related by

$$\dot{\epsilon} = \frac{2}{3} \frac{1}{\lambda^5} \frac{KD}{M}, \quad [1]$$

where M is the dislocation multiplication constant, K is a kinetic constant, λ is the characteristic dimension of the dislocation sub-structure. As for the creep strain rate $\dot{\epsilon}$ in nickel alloys strengthened by solid solution, Cannon and Sherby^[4] developed other formulas. When $EK' \gg AD\gamma^{3.5}\sigma^2$, $\dot{\epsilon}$ is given by

$$\dot{\epsilon} = \frac{AD\gamma^{3.5}\sigma^5}{E^5} \quad [2]$$

JUAN CHEN is with the Testing Center, Yangzhou University, Yangzhou, 225009 Jiangsu, P.R. China and also with the School of Chemistry and Chemical Engineering, Yangzhou University, Yangzhou, 225009 Jiangsu, P.R. China. LIJUN ZHANG is with the State Key Laboratory of Powder Metallurgy, Central South University, Changsha, 410083 Hunan, P.R. China. Contact e-mail: lijun.zhang@csu.edu.cn XIAO-GANG LU is with the School of Materials Science and Engineering, Shanghai University, Shanghai 200072, P.R. China.

Manuscript submitted August 1, 2018.

Article published online May 11, 2018

| | IIIB | IVB | VB | VIB | VIIB | VIII | IB | IIB | | |
|---|--------------------|--------------------|---------------------|--------------------|--------------------|--------------------|---------------------|--------------------|---------------------|--------------------|
| 4 | 21 Sc 44.956 | 22 Ti 47.90 | 23 V 50.942 | 24 Cr 51.996 | 25 Mn 54.938 | 26 Fe 55.847 | 27 Co 58.933 | 28 Ni 58.71 | 29 Cu 63.54 | 30 Zn 65.37 |
| 5 | 39 Y 88.905 | 40 Zr 91.22 | 41 Nb 92.906 | 42 Mo 95.94 | 43 Tc 99 | 44 Ru 101.07 | 45 Rh 102.905 | 46 Pd 106.4 | 47 Ag 107.870 | 48 Cd 112.40 |
| 6 | 57 La 138.91 | 72 Hf 178.49 | 73 Ta 180.948 | 74 W 183.85 | 75 Re 186.2 | 76 Os 190.2 | 77 Ir 192.2 | 78 Pt 195.09 | 79 Au 196.967 | 80 Hg 200.59 |

Fig. 1—(color on the web) Transition elements adjacent to Re for potential Re-substitutional elements in single-crystal Ni-based superalloys.

Table I. List of Terminal Compositions of the Diffusion Couples in the Present Work

| Couple No. | Composition (Wt Pct) | Temperature (K) | Diffusion Time (ks) |
|------------|-----------------------|-----------------|---------------------|
| ReC1 | Ni-2.32 Al/Ni-13.8 Re | 1473 | 500.4 |
| ReC2 | Ni/Ni-3.28 Al-8.85 Re | 1473 | 500.4 |
| ReC3 | Ni/Ni-1.75 Al-11.2 Re | 1473 | 500.4 |
| ReC4 | Ni-2.26 Al/Ni-14.0 Re | 1523 | 172.8 |
| ReC5 | Ni/Ni-3.18 Al-8.99 Re | 1523 | 172.8 |
| ReC6 | Ni/Ni-1.61 Al-14.6 Re | 1523 | 172.8 |
| ReC7 | Ni-2.23 Al/Ni-13.7 Re | 1573 | 111.72 |
| ReC8 | Ni/Ni-3.38 Al-8.70 Re | 1573 | 111.72 |
| ReC9 | Ni/Ni-1.69 Al-11.4 Re | 1573 | 111.72 |
| OsC1 | Ni/Ni-0.90 Al-8.52 Os | 1423 | 499.5 |
| OsC2 | Ni-1.31 Al/Ni-8.18 Os | 1473 | 500.4 |
| OsC3 | Ni/Ni-1.79 Al-5.56 Os | 1473 | 500.4 |
| OsC4 | Ni/Ni-0.88 Al-8.58 Os | 1473 | 500.4 |
| OsC5 | Ni-1.33 Al/Ni-8.07 Os | 1523 | 172.8 |
| OsC6 | Ni/Ni-1.75 Al-5.48 Os | 1523 | 172.8 |
| OsC7 | Ni/Ni-0.89 Al-8.85 Os | 1523 | 172.8 |
| OsC8 | Ni-1.32 Al/Ni-8.05 Os | 1573 | 25.32 |
| OsC9 | Ni/Ni-1.75 Al-5.61 Os | 1573 | 25.32 |
| OsC10 | Ni/Ni-0.89 Al-7.86 Os | 1573 | 25.32 |
| IrC1 | Ni-3.75 Al/Ni-21.9 Ir | 1423 | 499.5 |
| IrC2 | Ni/Ni-3.49 Al-14.8 Ir | 1423 | 499.5 |
| IrC3 | Ni/Ni-1.62 Al-17.0 Ir | 1423 | 499.5 |
| IrC4 | Ni-3.97 Al/Ni-21.7 Ir | 1473 | 500.4 |
| IrC5 | Ni/Ni-3.45 Al-16.0 Ir | 1473 | 500.4 |
| IrC6 | Ni/Ni-1.59 Al-17.3 Ir | 1473 | 500.4 |
| IrC7 | Ni-3.80 Al/Ni-22.2 Ir | 1523 | 172.8 |
| IrC8 | Ni/Ni-3.31 Al-14.8 Ir | 1523 | 172.8 |
| IrC9 | Ni/Ni-1.60 Al-17.9 Ir | 1523 | 172.8 |
| IrC10 | Ni/Ni-3.37 Al-14.4 Ir | 1573 | 25.32 |

with K' given as

$$K' = \frac{0.33kTD}{b^5e^2c}, \quad [3]$$

where A is a constant, D is the diffusion coefficient, and γ is the stacking fault energy, σ is stress, E is Young's modulus, k is the Boltzmann constant, T is the absolute temperature, b is the length of the Burgers vector, c is the concentration of the solute atom, and e is the fractional size difference between the solute and solvent atoms. When $EK' \ll AD\gamma^{3.5}\sigma^2$, $\dot{\epsilon}$ is represented by

$$\dot{\epsilon} = \frac{0.33kTD\sigma^3}{b^5e^2cE^4}. \quad [4]$$

Based on Eqs. [1] through [4], the creep strain rate $\dot{\epsilon}$ is proportional to the diffusion coefficient D of pure nickel or nickel alloys strengthened by solid solution. Therefore, one of the ways to improve creep resistance is to prepare SX Ni-based superalloys with as the low diffusion coefficients as possible.

Re, with very low diffusion coefficient, seems an optimal choice to enhance the creep resistance of Ni-based superalloys. The additional amount of Re increases from 3 wt pct for 2nd generation SX Ni-based superalloys to 6 wt pct for 3rd generation alloys. Although the additional amount of Re effectively enhances creep resistance of Ni-based superalloys, some side effects also occur.^[5] On one hand, more additional

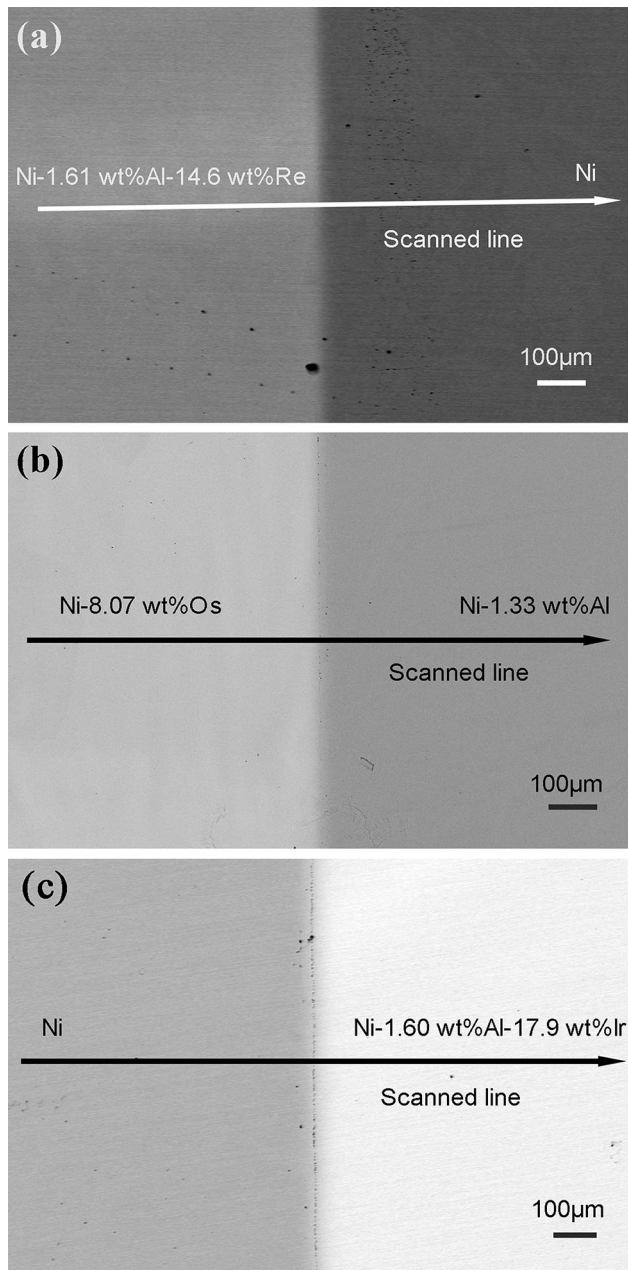


Fig. 2—(color on the web) Backscattered electronic images of (a) ReC6; (b) OsC5; (c) IrC9 diffusion couples in this work.

amount of Re is prone to formation of brittle topologically packed phases (TCPs), on the other hand, Re is expensive, and more additional amount will increase the cost of SX Ni-based superalloys. These drawbacks have inspired intensive research to search suitable Re replacements in superalloys.^[5–11]

According to Eqs. [1] through [4], it is wise to search for potential alloying elements to substitute for Re based on diffusion coefficients, such as by comparing the diffusion coefficients of different elements with those of Re without considering the cost of such elements. The adjacent elements to Re in the periodic table depicted in Figure 1 (e.g., Ti, Co, Ni, Nb, Mo, Ru, Rh, Ta, W, Os,

Ir, and Pt) are considered first as potential substitutes for Re. Some researchers recently calculated the impurity diffusivities of different alloying elements in pure nickel;^[5,9,11,12] however, the composition- and temperature-dependent interdiffusivities of alloying elements in face-centered cubic (fcc) matrix, which are also influenced by the composition gradient of other elements, should be used in more suitable quantities to account for actual service situations. Therefore, it is necessary to measure the accurate composition- and temperature-dependent interdiffusivity matrices of different alloying elements in SX Ni-based superalloys. In the very recent work from our group, we measured the composition- and temperature-dependent interdiffusion coefficients in fcc Ni-X (X = Rh, Ta, W, Re, and Ir) alloys and compared interdiffusivities in binary Ni-TM (here, TM denotes 3d, 4d, and 5d transition metal elements) systems with those in the binary Ni-Re system.^[13] The results show that fcc Ni-6 wt pct Os alloys, Ni-6 wt pct Re, and Ni-6 wt pct Ir alloys are arranged in order of interdiffusivity from smallest to largest. Here, the additional amount of 6 wt pct is chosen because the additional amount of Re in 3rd generation Ni-based superalloys is 6 wt pct.

In typical Ni-based single-crystal superalloys, 10 or even more different alloying elements are included. Al, as the element to form the important L1₂ (Ni₃Al) precipitation phase, is an essential alloying element in Ni-based single-crystal superalloys. To find a replacement for Re in practical SX Ni-based superalloys, it is essential to further explore the interdiffusivities in fcc ternary or higher-order Ni-Al-based alloys. Research on ternary systems is thus to be performed in the present work, a further investigation on quaternary and high-order systems will be conducted in a subsequent study.

The elements involved in this work are marked in Figure 1. Interdiffusivity information is available in the literature for fcc Ni-Al-X (X = Ti, Co, Ni, Nb, Mo, Ru, Rh, Ta, W, and Pt) alloys.^[14–22] However, no interdiffusivity information has existed regarding fcc Ni-Al-Os and Ni-Al-Ir systems until now. In previous research,^[13] Os and Ir were found to be the slow diffusers, and no report has demonstrated that they tend to form TCP phases. Thus, the experimental interdiffusivity data need to be measured for these two systems. Moreover, as for the fcc Ni-Al-Re system, only diffusivities at several specific concentration points are available.^[19,23,24] To obtain more data on interdiffusivities for the core Ni-Al-Re system, more interdiffusivities in the fcc Ni-Al-Re system will also be evaluated in the present work.

Typically, the Matano–Kirkaldy (M–K) method, together with single-phase diffusion couples experiments, is a common method to evaluate ternary interdiffusion coefficients. However, this traditional method is of low efficiency. To improve the situation, a pragmatic numerical inverse method^[25,26] was proposed by our research group, which efficiently measured composition-dependent interdiffusivities along the entire diffusion paths of diffusion couples. Furthermore, a powerful software, HitDIC (High-Throughput Determination of Interdiffusion Coefficients),^[27,28] was

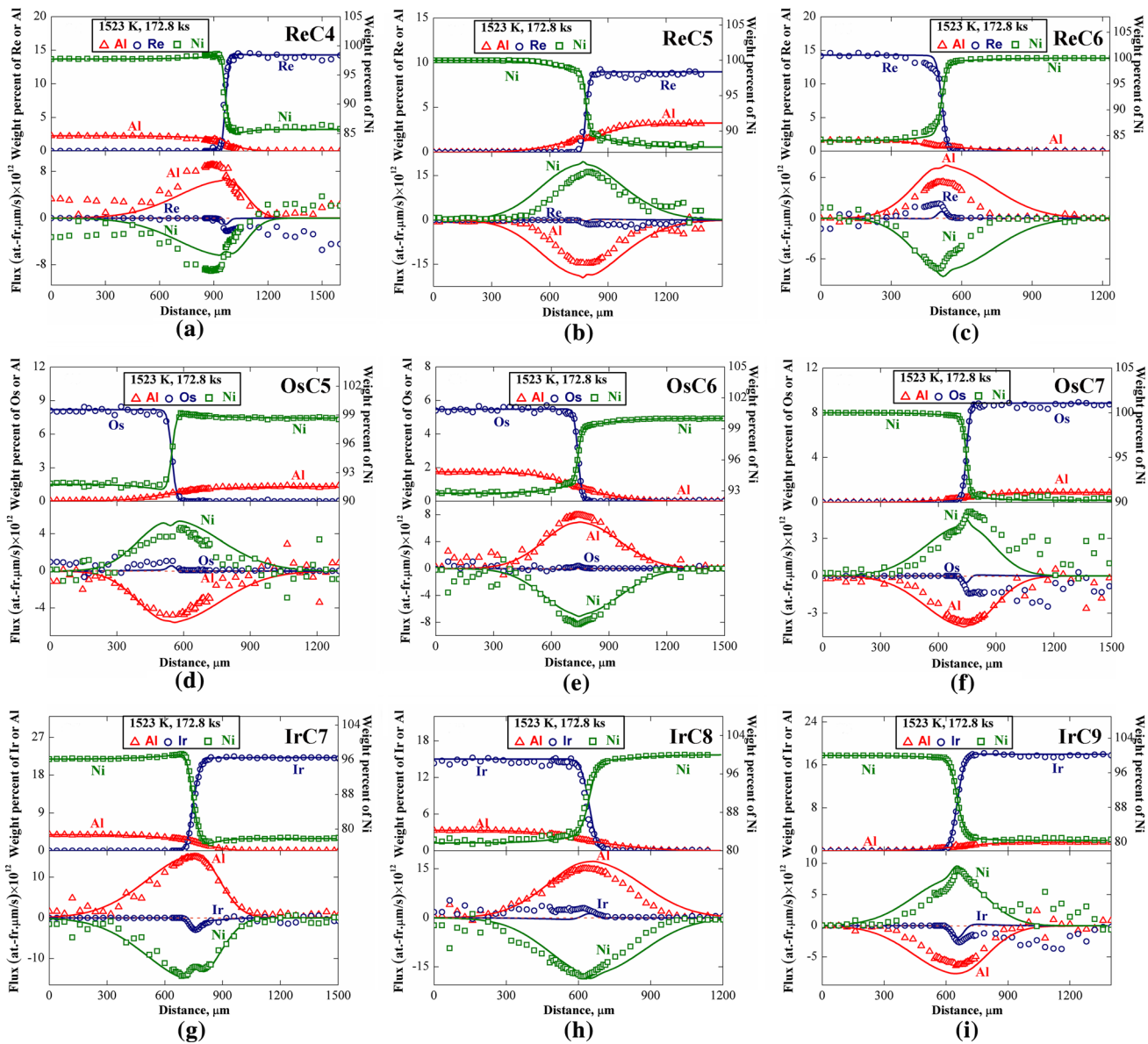


Fig. 3—(color on the web) Experimental/model-predicted concentration profiles and interdiffusion flux profiles for (a) ReC4; (b) ReC5; (c) ReC6; (d) OsC5; (e) OsC6; (f) OsC7; (g) IrC7; (h) IrC8; (i) IrC9 diffusion couples annealed at 1523 K for 172.8 ks.

recently realized to automate calculation procedures based on the proposed numerical inverse method.

Consequently, the primary objectives in this work are (i) to measure the composition- and temperature-dependent interdiffusion coefficients of fcc Ni-Al-X (X = Re, Os, and Ir) alloys at 1423 K to 1573 K by using HitDIC software in the numerical inverse method framework together with the single-phase ternary diffusion couple technique, and validate their reliability; and (ii) to fully compare the interdiffusivities of fcc Ni-Al-X (X = TM) alloys with those of fcc Ni-Al-Re alloys at the typical composition for Re in commercial SX Ni-based alloys and further analyze the factors including alloying element concentration, atomic number, atomic radius,

and activation energy that influence interdiffusion coefficient values, from which potential Re substitutes can be proposed for next-generation Ni-based superalloys.

II. EXPERIMENTAL PROCEDURE

High-purity Ni ingots (99.99 wt pct), high-purity Al ingots (99.99 wt pct), high-purity Re pieces (99.99 wt pct), high-purity Os pieces (99.99 wt pct), and high-purity Ir particles (99.99 wt pct) were mixed in the proportions listed in Table I to prepare alloys. The preparation processes of the diffusion couples in Table I were introduced step by step. All alloys were prepared

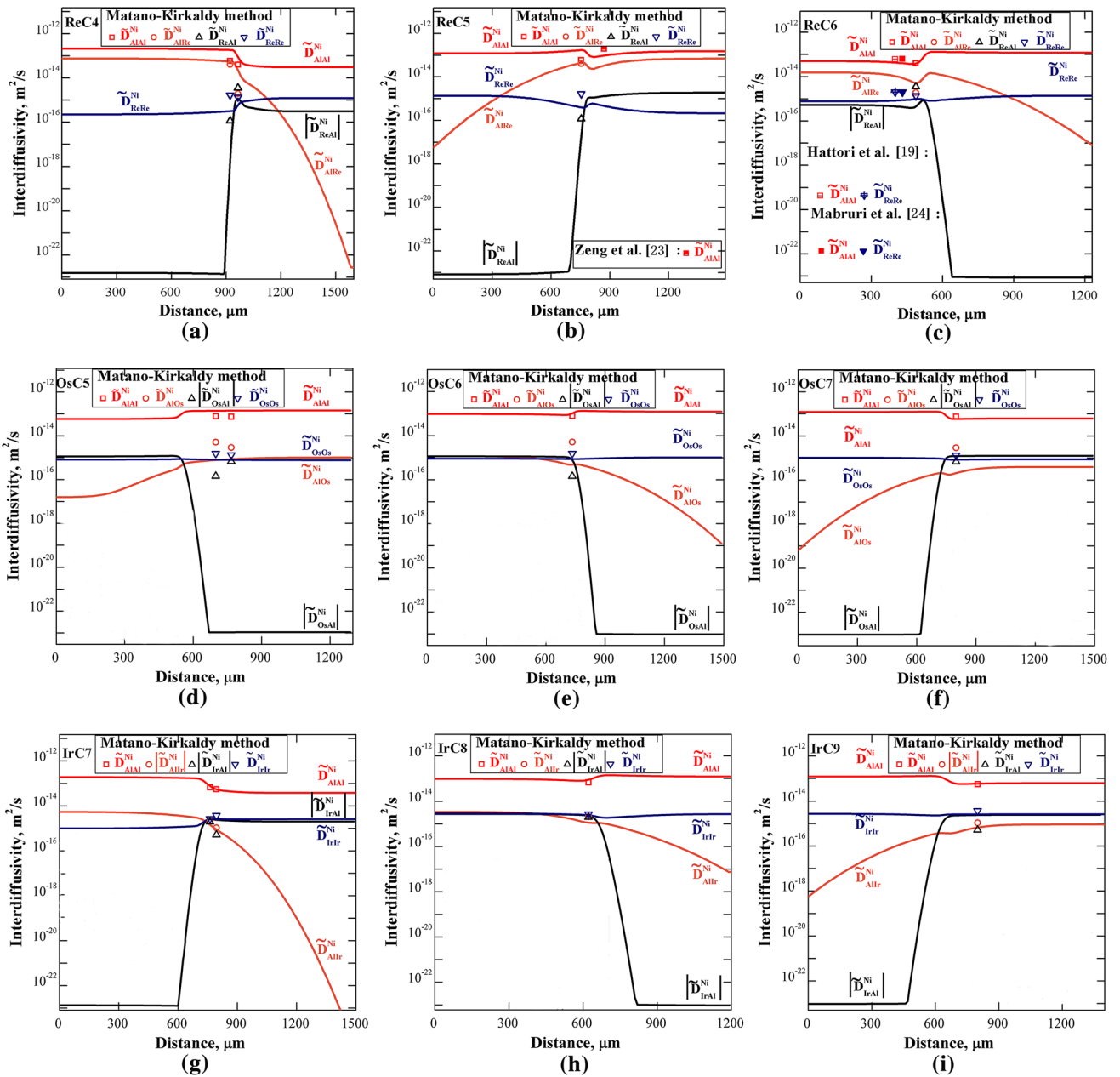


Fig. 4—(color on the web) Interdiffusivities along the entire diffusion paths for (a) ReC4; (b) ReC5; (c) ReC6; (d) OsC5; (e) OsC6; (f) OsC7; (g) IrC7; (h) IrC8; (i) IrC9 diffusion couples evaluated by the numerical inverse method and Matano–Kirkaldy method at 1523 K.

using arc melting in an argon atmosphere (WKDHL-1, Opto-electronics Co. Ltd., Beijing, China). The prepared alloys were sealed into respective vacuum quartz tubes and homogenized at 1573 ± 2 K for 288 ks (80 hours). After being quenched in water, all alloys were subjected to X-ray diffraction (XRD) analysis to confirm their location in single fcc phase region. All buttons were cut into appropriately sized blocks of $5 \times 5 \times 1.5$ mm³, which were then ground and carefully polished. Diffusion couples were assembled using Mo clamps to bind the polished surfaces of two alloy samples.

The diffusion couples were encapsulated using vacuum quartz tubes and followed by annealing at 1423 ± 2 , 1473 ± 2 , and 1523 ± 2 K for 499.5, 500.4, and 172.8 ks, respectively, before water quenching. The annealing times differed for the samples of the three ternary systems annealed at 1573 ± 2 K, 111.72 ks for Ni–Al–Re system, and 25.32 ks for Ni–Al–Os and Ni–Al–Ir systems. After diffusion annealing, the plane of diffusion couples parallel to the diffusion direction were cut and further polished. The concentration profiles from the above diffusion couples were obtained using an electron probe

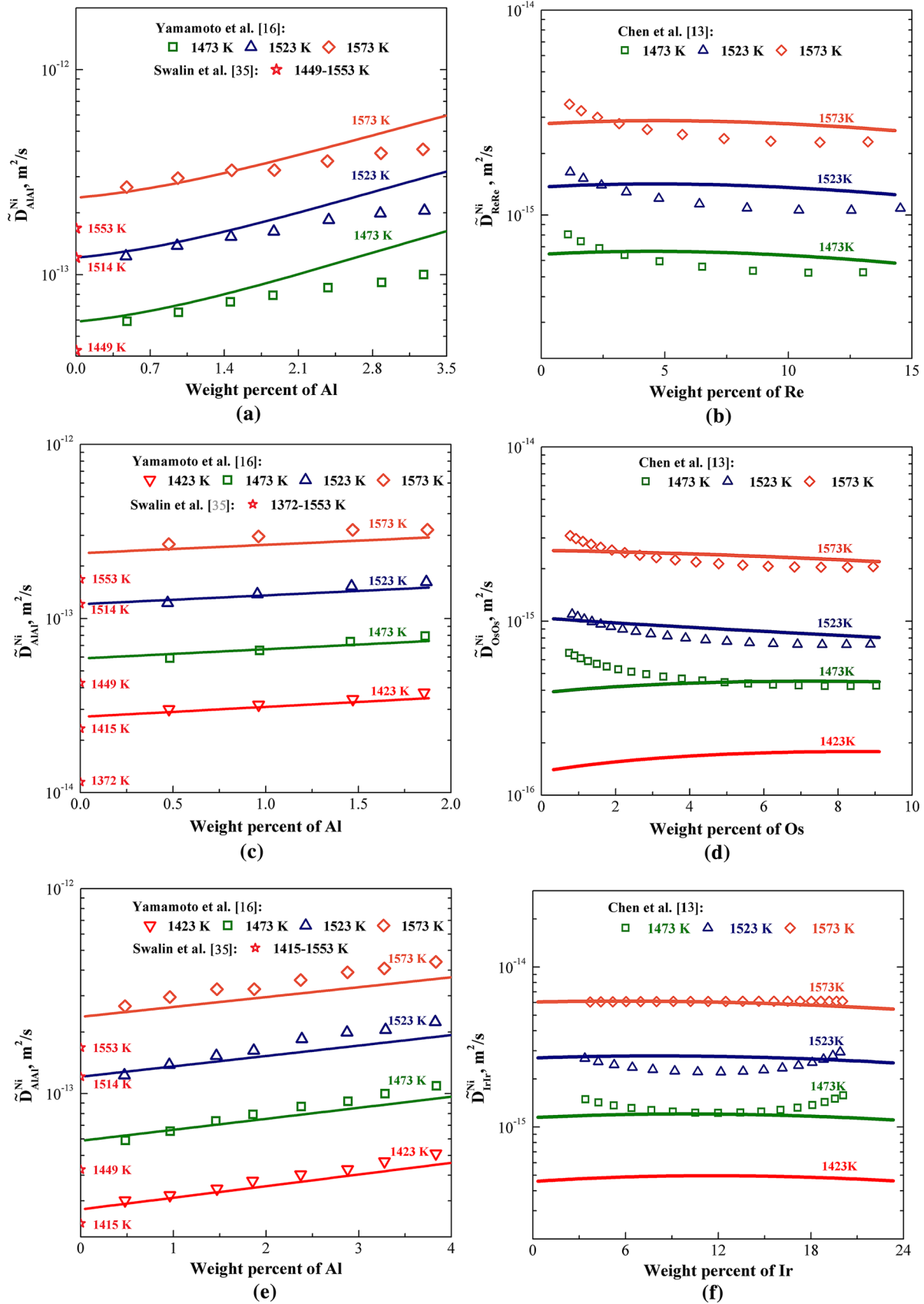


Fig. 5—(color on the web) Extrapolated interdiffusivities for (a) Ni-Al and (b) Ni-Re boundary binaries in the Ni-Al-Re system, (c) Ni-Al and (d) Ni-Os boundary binaries in the Ni-Al-Os system, (e) Ni-Al and (f) Ni-Ir boundary binaries in the Ni-Al-Ir system by using the numerical inverse method.

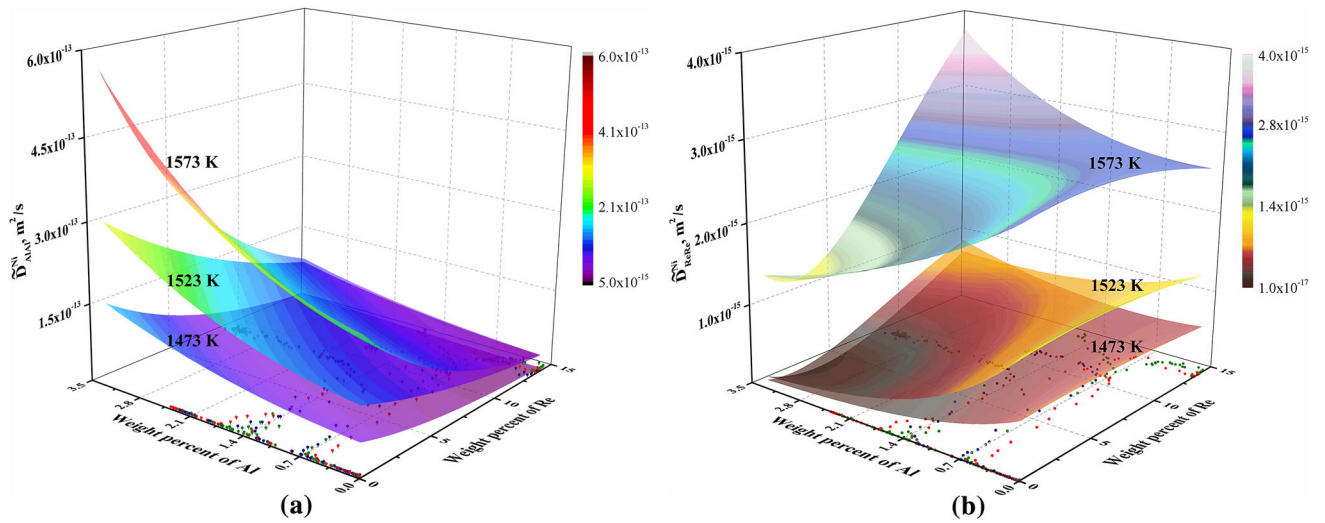


Fig. 6—(color on the web) Main interdiffusivity surfaces for (a) \bar{D}_{AlAl}^{Ni} and (b) \bar{D}_{ReRe}^{Ni} varied with Al and Re contents in ternary fcc Ni-Al-Re system at 1473 K, 1523 K, and 1573 K.

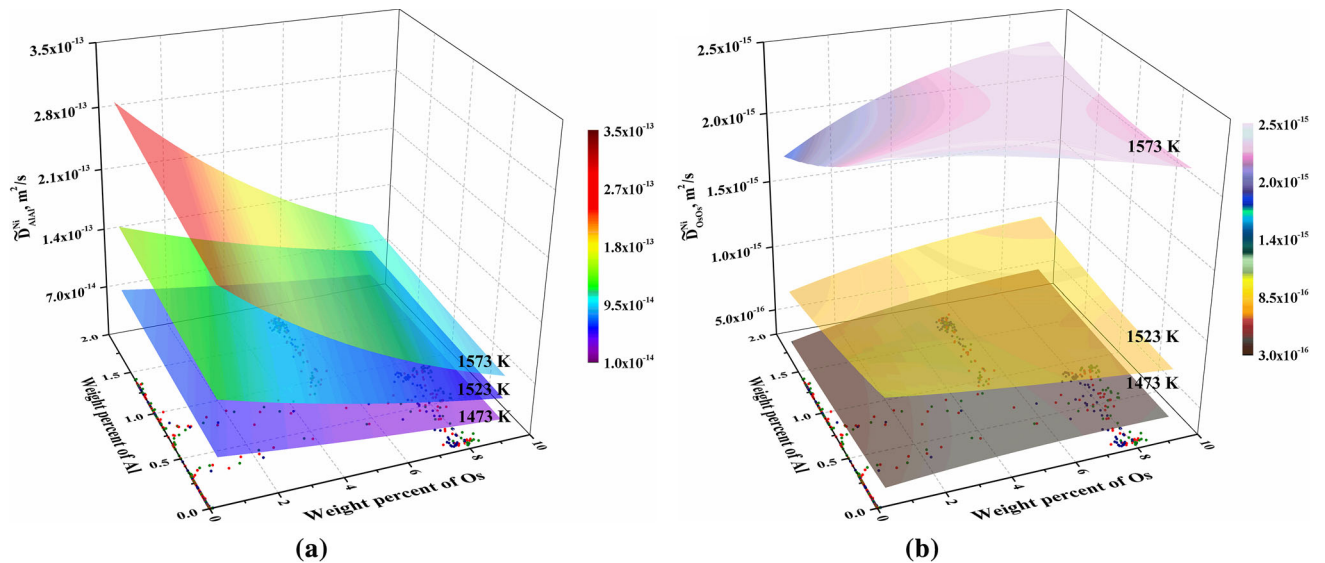


Fig. 7—(color on the web) Main interdiffusivity surfaces for (a) \bar{D}_{AlAl}^{Ni} and (b) \bar{D}_{OsOs}^{Ni} varied with Al and Os contents in ternary Ni-Al-Os system at 1473, 1523, and 1573 K.

micro-analyzer (EPMA) (JXA-8100, JEOL, Japan) along the diffusion direction. The error from the component determination is typically within 1 pct.

III. RESULTS AND DISCUSSION

Typical backscattered electron images (BEIs) of ReC6 (Ni/Ni-1.61 Al-14.6 Re), OsC5 (Ni-1.33 Al/Ni-8.07 Os), and IrC9 (Ni/Ni-1.60 Al-17.9 Ir) diffusion couples annealed at 1523 K are shown in Figure 2 revealing the following: (i) end-member alloys were located in the single-phase region, (ii) good connections between the alloys for the three diffusion couples were achieved, and (iii) diffusion zones form in the central region between end-member alloys. The typical experimental

concentration profiles of ReC4, ReC5, ReC6, OsC5, OaC6, OsC7, IrC7, IrC8, and IrC9 (marked by symbols) annealed for 172.8 ks (48 hours) at 1523 K are displayed in Figure 3. As shown in Figure 3(a), (d), and (g), the uphill diffusion of Ni occurs in Ni-Al/Ni-X- type diffusion couples, potentially attributable to the effects of refractory elements (*i.e.*, Re, Os, and Ir). Similar uphill diffusion has also been identified in Ni-Al-Ta and Ni-Al-Pt systems.^[21,22] Based on the concentration profiles of all components in each diffusion couple, the corresponding experimental interdiffusion fluxes were evaluated using the Dayananda approach^[29] and are presented with symbols in Figure 3. The profiles of Al have gentler slopes than those of Ni, Re, Os, and Ir, indicating Al diffuses faster than Ni, Re, Os, and Ir, this is quite common.

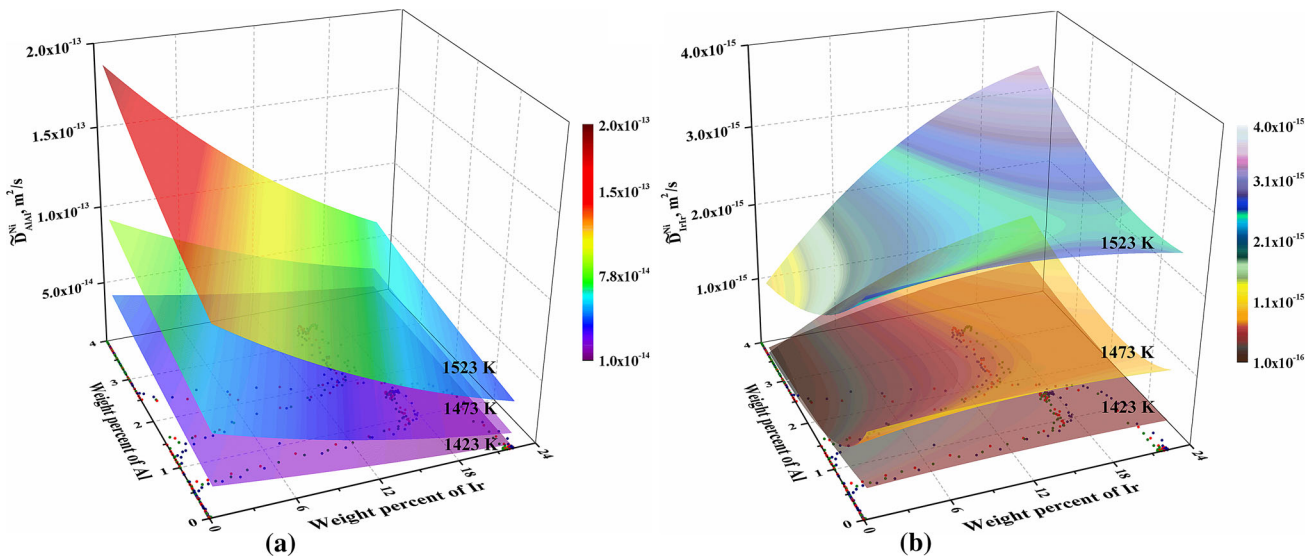


Fig. 8—(color on the web) Main interdiffusivity surfaces for (a) \bar{D}_{AlAl}^{Ni} and (b) \bar{D}_{IrIr}^{Ni} varied with Al and Ir contents in ternary Ni-Al-Ir system at 1423 K, 1473 K, and 1523 K.

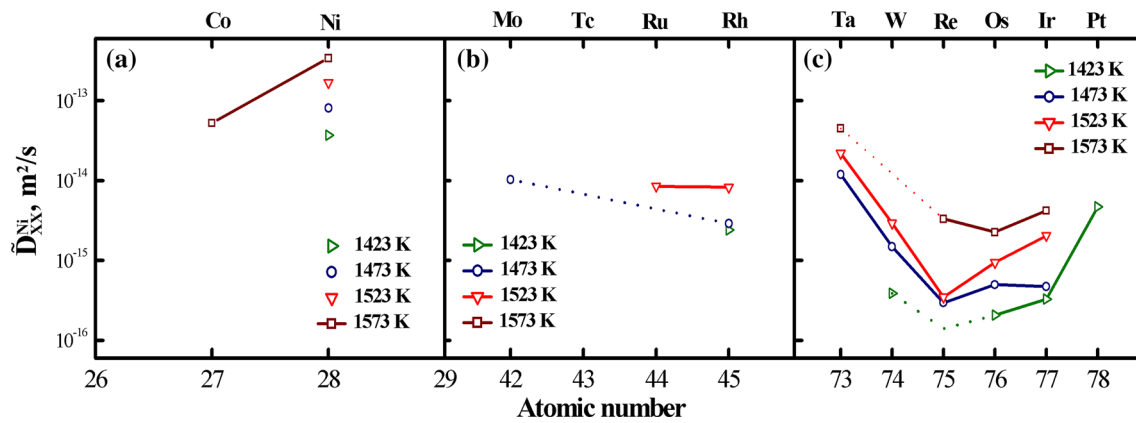


Fig. 9—(color on the web) Variation of the interdiffusion coefficients for (a) 3d, (b) 4d, and (c) 5d transition elements in fcc Ni-2 wt pct Al-6 wt pct X (X = Co, Ni, Mo, Ru, Rh, Ta, W, Re, Os, Ir, and Pt) at 1423 K to 1573 K in this work and the literature^[18, 20–25] by atomic number.

Table II. Comparison of the Interdiffusivities \bar{D}_{XX}^{Ni} in Ni-Al-X (X = Nb and Ti) and \bar{D}_{ReRe}^{Ni} in Ni-Al-Re Alloys

| Composition (Wt Pct) | | \bar{D}_{XX}^{Ni} (10^{-15} m ² /s) | Temperature (K) | Alloys | References |
|----------------------|------|--|-----------------|----------|------------|
| Al | X | | | | |
| 1.62 | 3.97 | 24.2 | 1473 | Ni-Al-Nb | 17 |
| 1.62 | 3.97 | 0.26 | 1473 | Ni-Al-Re | this work |
| 1.30 | 2.39 | 36.8 | 1473 | Ni-Al-Nb | 17 |
| 1.30 | 2.39 | 0.28 | 1473 | Ni-Al-Re | this work |
| 1.32 | 1.81 | 75 | 1473 | Ni-Al-Ti | 14 |
| 1.32 | 1.81 | 0.25 | 1473 | Ni-Al-Re | this work |
| 1.96 | 2.51 | 81.6 | 1473 | Ni-Al-Ti | 14 |
| 1.96 | 2.51 | 0.17 | 1473 | Ni-Al-Re | this work |

As stated in Section I, HitDIC software^[27] developed using numerical inverse method framework^[25,26] was utilized to extract interdiffusion coefficients along entire diffusion paths based on the experimental profiles of fcc

Ni-Al-X (X = Re, Os, and Ir) systems. The thermodynamic descriptions for Ni-Al-Re systems have been reported^[30] and were considered when evaluating the interdiffusivities of the fcc Ni-Al-Re system. In fact,

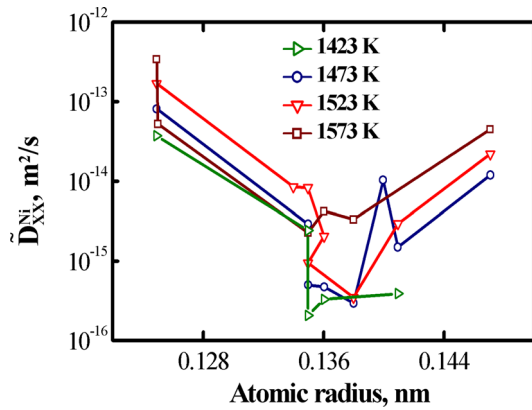


Fig. 10—(color on the web) Variation of the interdiffusivities in Ni-2wt pct Al-6wt pct X (X = Co, Ni, Mo, Ru, Rh, Ta, W, Re, Os, Ir, and Pt) alloys by atomic radius at 1423 K to 1573 K.

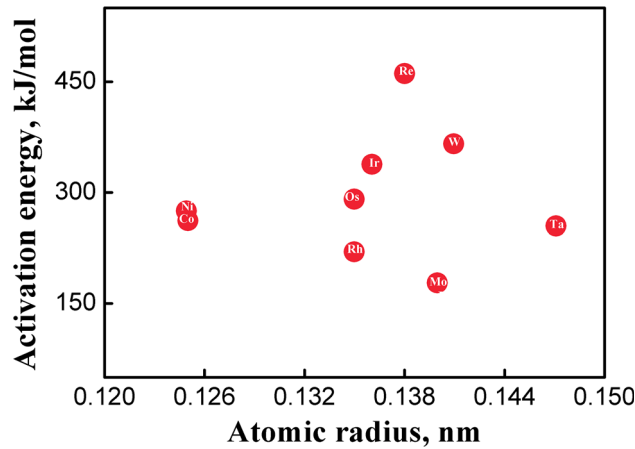


Fig. 11—(color on the web) Measured activation energies varied with the atomic radius.

whether reliable thermodynamic descriptions of the target alloy system were used during evaluation has a negligible influence on final interdiffusivities.^[26] Actually, in the spirit of the proposed numerical inverse method,^[25–28] the quality of obtained interdiffusivities is only determined by the degree of fit of model-predicted concentration/interdiffusion flux profiles to the experimental ones. The accuracy of the thermodynamic factor only affects the values of the fitting parameters, but not the reliability of the final interdiffusivities, thus, the proposed numerical inverse method remains applicable in the case without reliable thermodynamic description for the target alloy. In this case, thermodynamic factors and mobility parameters in the numerical inverse method are only treated as numerical parameters without any physical meaning.

Moreover, for Ni–Al–Os and Ni–Al–Ir systems, no self-consistent thermodynamic database is available. Therefore, the fcc phase in the Ni–Al–Os and Ni–Al–Ir systems were simply assumed to be the ideal solution. The interdiffusivity matrices in each ternary system were evaluated by achieving the best fit between

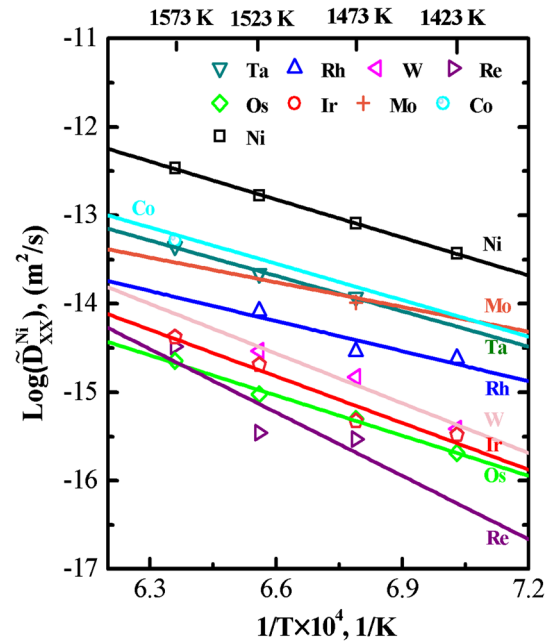


Fig. 12—(color on the web) Temperature-dependent interdiffusivities in Ni-2wt pct Al-6wt pct X (X = Co, Ni, Mo, Ru, Rh, Ta, W, Re, Os, Ir, and Pt) alloys.

the experimental and simulated concentration and interdiffusion curves. Only the evaluated interdiffusivities fulfilling the thermodynamically stable constraints^[31] were considered to be reliable and used as the final results.

The evaluated concentration-dependent interdiffusivities \tilde{D}_{AlAl}^{Ni} , \tilde{D}_{AlX}^{Ni} , \tilde{D}_{XAl}^{Ni} , and \tilde{D}_{XX}^{Ni} for all fcc Ni–Al–X (X = Re, Os, and Ir) diffusion couples at 1523 K are presented in Figure 4. \tilde{D}_{AlAl}^{Ni} and \tilde{D}_{XX}^{Ni} are the main interdiffusivities of Al and X, which present the diagonal terms in the ternary interdiffusivity matrix. While \tilde{D}_{AlX}^{Ni} and \tilde{D}_{XAl}^{Ni} are the cross ones, which denote the non-diagonal terms. Moreover, all evaluated interdiffusivities for Ni–Al–X (X = Re, Os, and Ir) systems in the present work at all temperatures were collected in the electronic Supplementary Materials A1. Meanwhile, the mobility parameters of the Ni–Al–X (X = Re, Os, and Ir) system evaluated when calculating the interdiffusivities using HitDIC were also summarized in the electronic Supplementary Materials A2 to meet the needs of readers. All main interdiffusivities are positive, but the cross interdiffusivities are either negative or positive. Absolute values of negative cross interdiffusivities are marked in Figure 4. Moreover, the error propagation method proposed by L echelle *et al.*^[32] was used to acquire the errors of the evaluated interdiffusivities. The average relative errors of the interdiffusivities \tilde{D}_{AlAl}^{Ni} , \tilde{D}_{AlX}^{Ni} , \tilde{D}_{XAl}^{Ni} , and \tilde{D}_{XX}^{Ni} were as follows: 26.3, 26.6, 24.6, and 24.8 pct in fcc Ni–Al–Re system, 20.5, 19.3, 37.4, and 40.5 pct in fcc Ni–Al–Os system, 19.9, 37.0, 50.0, and 36.8 pct in fcc Ni–Al–Ir system, respectively. Figure 4 shows that the main interdiffusivity \tilde{D}_{AlAl}^{Ni} is generally larger than \tilde{D}_{XX}^{Ni} ,

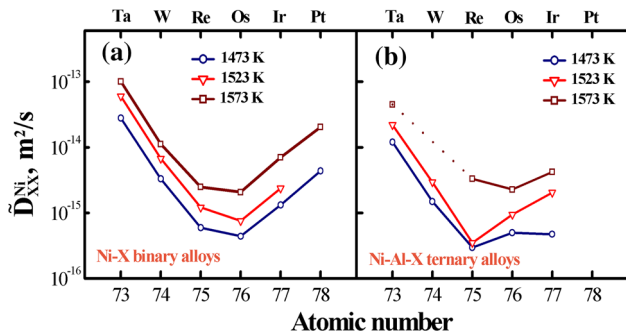


Fig. 13—(color on the web) Variation trends of interdiffusivities in (a) binary and (b) ternary systems. The data in (a) are originated from our previous publication.^[13]

supporting the slopes of the concentration profiles for Re, Os, and Ir as being much steeper than those for Al.

The evaluated interdiffusivities for fcc Ni-Al-X (X = Re, Os, and Ir) system are verified in four aspects. While evaluating the interdiffusion coefficients *via* HitDIC software, the composition profiles and computed interdiffusion fluxes were obtained simultaneously. The experimental and simulated concentration profiles and interdiffusion fluxes are displayed in Figure 2, reflecting satisfactory agreement between the simulated and experimental concentration profiles. Slight deviations appear between the computed and experimental interdiffusion fluxes presumably due to the following reasons: (i) the experimental interdiffusion fluxes were evaluated on the basis of raw experimental concentration data with certain scattering, and the small degree of scattering in the concentration data may result in relatively large scattering in interdiffusion fluxes (*i.e.*, gradient of concentration profiles), especially for those exhibiting a complex up-hill diffusion phenomenon; and (ii) only one set of mobility parameters was utilized for three diffusion couples at one temperature, which may cause local deviations.

The interdiffusivities extracted by the traditional M–K method^[33,34] are also superimposed in Figure 4 and compared with the results derived by HitDIC software. Figure 4 shows reasonable agreement on the interdiffusivities obtained by the two methods. As mentioned in the introduction, Hattori *et al.*,^[19] Zeng *et al.*,^[23] and Maburri *et al.*^[24] studied interdiffusivities in the fcc Ni-Al-Re system, and the corresponding data are superimposed in Figures 4(b) through (c) for direct comparison with the presently derived values. The experimental data in the literature are close to the measured values in the current study. In the phase diagram, when the X concentration approaches 0, the \tilde{D}_{AlAl}^{Ni} in the ternary Ni-Al-X system should approach the \tilde{D}_{AlAl}^{Ni} in binary Ni-Al system. When the Al concentration approaches 0, the \tilde{D}_{XX}^{Ni} in ternary Ni-Al-X system should approach the \tilde{D}_{XX}^{Ni} in binary Ni-X system. When the X concentration is equal to 0 and the Al concentration approaches 0, the \tilde{D}_{AlAl}^{Ni} in ternary Ni-Al-X system should approach the impurity Al in fcc Ni in binary Ni-Al system.

We also conducted comparisons among the calculated interdiffusivities using the numerical inverse method in the boundary binary Ni-Al and Ni-X systems and experimental data in the binary systems measured using Sauer–Friese method^[13,16] and impurity diffusivities.^[35] Results are presented in Figure 5 depicting an acceptable fit between the calculated and experimental results. Therefore, the present interdiffusivities extracted from the numerical inverse method are reliable.

Three-dimensional (3-D) interdiffusivity surfaces can be drawn based on composition-dependent interdiffusivities at 1423 K to 1573 K in Ni-Al-X (X = Re, Os, and Ir) system and are presented in Figures 6, 7, and 8. The 3-D surfaces over such a wide compositional range at different temperatures are helpful for understanding variation trends in different interdiffusivities. The plots of \tilde{D}_{AlAl}^{Ni} and \tilde{D}_{XX}^{Ni} generally increase as the temperature increases, and the increments of \tilde{D}_{XX}^{Ni} are larger than those of \tilde{D}_{AlAl}^{Ni} in the higher temperature region. Moreover, \tilde{D}_{AlAl}^{Ni} increases as the Al concentration increases, and decreases as the X concentration increases. \tilde{D}_{XX}^{Ni} increases roughly with an increase in both Al and X concentrations.

IV. SCREENING OF POSSIBLE RE-SUBSTITUTIONAL ELEMENTS

In 3rd generation Ni-based superalloys, additional amounts of Re and Al are 6 and 0.5 to 7.4 wt pct,^[36–38] respectively. To make a reasonable comparison, the interdiffusion coefficients at the same alloy composition with 2 wt pct Al and 6 wt pct X were selected. Possible Re-substitutional elements in SX Ni-base superalloys focus on 3d, 4d, and 5d elements, including Ti, Co, Ni, Nb, Mo, Ru, Rh, Ta, W, Os, Ir, and Pt. In Figure 9, the main interdiffusivities \tilde{D}_{XX}^{Ni} in Ni-2 wt pct Al-6 wt pct X alloys (X = Co,^[15] Ni,^[16] Mo,^[18] Ru,^[19] Rh,^[20] Ta,^[21] W,^[20] Re, Os, Ir, and Pt^[22]) are taken directly from either the literature or the present work. Notably, in Figure 9, the interdiffusivities \tilde{D}_{XX}^{Ni} for some elements at several temperatures are still absent due to a lack of experimental information in the literature. Figure 9 indicates that the diffusion rates of 5d solutes are generally lower than those of 3d and 4d solutes. Moreover, interdiffusivities of elements in the middle of the row are generally lower for 5d elements than for other elements shown in Figure 9(c). The most important information from Figure 9 is that Re exhibits the lowest diffusion rate at 1473 K and 1523 K, followed by Os and Ir, whereas Os represents the lowest rate at 1573 K, followed by Re and Ir.

For Nb and Ti, the interdiffusivities \tilde{D}_{XX}^{Ni} in Ni-2 wt pct Al-6 wt pct X alloys are still lacking in the literature. Thus, their diffusion rates at other compositions are also compared with those of Re, as illustrated in Table II. The diffusivities \tilde{D}_{XX}^{Ni} of Ni-Al-Nb alloys are 93 to 131 times larger than those of Ni-Al-Re alloys, and the diffusivities \tilde{D}_{XX}^{Ni} of Ni-Al-Ti alloys are 300 to 480 times larger than those of Ni-Al-Re alloys given in

Table II. Therefore, the diffusion rates of Nb and Ti are much higher than that of Re.

Figure 10 displays the interdiffusivities in Ni-2 wt pct Al-6 wt pct X (X = Co,^[15] Ni,^[16] Mo,^[18] Ru,^[19] Rh,^[20] Ta,^[21] W,^[20] Re, Os, Ir, and Pt^[22]) alloys against atomic radius at 1423 K to 1573 K. As shown, the interdiffusion coefficients for Ni-2wt pct Al-6wt pct X alloys first decrease and then increase with an increasing atomic radius. The interdiffusivities exhibit lower values when the atomic radius ranges from 0.134 to 0.138 nm, however, an abnormality appears for interdiffusivities when the atomic radius is 0.14 nm, and the corresponding element is Mo. The reason for such abnormality requires further investigation. Figure 11 describes the relationship between the atomic radius and activation energy, and activation energies are obtained from Figure 12. In general, activation energy increases first, peaks at Re, and then declines as the atomic radius increases—except for the element Mo, which has abnormally small activation energy. The variation trend of activation energy is generally consistent with that of interdiffusivity.

Figure 12 presents the temperature-dependent interdiffusivities of Ni-2wt pct Al-6wt pct X (X = Co, Ni, Mo, Ru, Rh, Ta, W, Re, Os, Ir, and Pt) alloys. Ni, Mo, Ta, Rh, and W have larger diffusion rates than Ir, Os, and Re, as depicted in Figure 9. The diffusion rate of Os is smaller than that of Ir at 1423 K to 1573 K, while the diffusion rate difference between Os and Ir becomes larger as the temperature continues to increase. The diffusion rate of Re is smaller than that of Os when the temperature is below 1573 K, while the diffusion rate of Os becomes smaller than that of Re when the temperature is above 1573 K. Similarly, the diffusion rate difference between Re and Os becomes larger as the temperature continues to rise.

As mentioned above, diffusion rates of Os and Ir in ternary fcc Ni-2 wt pct Al-6 wt pct X alloys are the closest to the diffusion rate of Re among the screened 3d, 4d, and 5d elements. Moreover, Os has an even lower diffusion rate than Re when the temperature exceeds 1573 K. In direct contrast with the conclusion from binary alloys, the interdiffusivities $\tilde{D}_{XX}^{\text{Ni}}$ in binary Ni-6wt pct X alloys^[13] and ternary Ni-2wt pct Al-6wt pct X alloys are shown in Figure 13. For binary systems displayed in Figure 13a, the diffusion rate of Os is always lower than that of Re at 1473 K to 1573 K. For ternary systems shown in Figure 13b, the diffusion rate of Re is lower than that of Os at 1473 K and 1523 K but is higher at 1573 K. The change may be due to the influence of the second alloying element Al.

V. CONCLUSIONS

- 29 diffusion couples for fcc Ni-Al-X (X = Re, Os, and Ir) systems at 1423 K to 1573 K were prepared and their concentration profiles were measured after diffusion annealing. Based on the measured composition profiles, high-throughput determination of

interdiffusivity matrices over the composition spaces was performed using HitDIC in the framework of the numerical inverse method.

- The reliability of the obtained interdiffusivities in the present work was fully verified through comparison with the calculated results of the M–K method, the experimental data of corresponding ternary systems in the literature, and the measured data in boundary binary systems and the impurity diffusivities.
- A comprehensive comparison was conducted among the interdiffusion coefficients/diffusion properties in fcc Ni-2 wt pct Al-6 wt pct X (X = Ti, Co, Ni, Nb, Mo, Ru, Rh, Ta, W, Re, Os, Ir, and Pt) alloys at 1423–1573 K, along with further analysis on variations in the interdiffusion coefficients with different influence factors.
- It is proposed that Os and Ir are potential substitutes for Re in new generation of Ni-based single-crystal superalloys in terms of diffusion coefficients.

ACKNOWLEDGMENTS

The financial support from the National Natural Science Foundation of China (Grant No. 51474239) and the Hunan Provincial Science and Technology Program of China (Grant No. 2017RS3002)—Huxiang Youth Talent Plan is acknowledged. Lijun Zhang acknowledges that the project was supported by the State Key Laboratory of Powder Metallurgy Foundation, Central South University, Changsha, China.

ELECTRONIC SUPPLEMENTARY MATERIAL

The online version of this article (<https://doi.org/10.1007/s11661-018-4669-1>) contains supplementary material, which is available to authorized users.

REFERENCES

1. S.H. Liu, M.R. Wen, Z. Li, W.Q. Liu, P. Yan, and C.Y. Wang: *Mater. Des.*, 2017, vol. 130, pp. 157–65.
2. X. Xiong, P. Dai, D. Quan, Z. Wang, Q. Zhang, and Z. Yue: *Mater. Des.*, 2015, vol. 86, pp. 482–86.
3. R.C. Reed: *The Superalloys: Fundamentals and Applications*, Cambridge University Press, Cambridge, 2006.
4. W.R. Cannon and O.D. Sherby: *Metall. Trans.*, 1970, vol. 1, pp. 1030–32.
5. C.L. Zacherl: A computational investigation of the effect of alloying elements on the thermodynamic and diffusion properties of fcc nickel alloys, with application to the creep rate of dilute nickel-X alloys, Doctoral thesis, Pennsylvania State University, 2012.
6. W.Y. Gong, L.J. Zhang, D.Z. Yao, and C.G. Zhou: *Scr. Mater.*, 2009, vol. 61, pp. 100–03.
7. M.J.H. Van Dal, M.C.L.P. Pleumeekers, A.A. Kodentsov, and F.J.J. Van Loo: *Acta Mater.*, 2000, vol. 48, pp. 385–96.
8. R.A. Hobbsa, M.S.A. Karunaratne, S. Tina, R.C. Reed, and C.M.F. Rae: *Mater. Sci. Eng. A*, 2007, vols. 460–461, pp. 587–94.
9. M.S.A. Karunaratne and R.C. Reed: *Acta Mater.*, 2003, vol. 51, pp. 2905–19.

10. M.S.A. Karunaratne, P. Carter, and R.C. Reed: *Mater. Sci. Eng. A*, 2000, vol. 281, pp. 229–33.
11. X.M. Zhang, H.Q. Deng, S.F. Xiao, Z. Zhang, J.F. Tang, L. Deng, and W.Y. Hu: *J. Alloys Compd.*, 2014, vol. 588, pp. 163–69.
12. A. Janotti, M. Krčmar, C.L. Fu, and R.C. Reed: *Phys. Rev. Lett.*, 2004, vol. 92, art. no. 085901.
13. J. Chen, J.K. Xiao, L.J. Zhang, and Y. Du: *J. Alloys Compd.*, 2016, vol. 657, pp. 457–63.
14. M.S.A. Karunaratne, P. Carter, and R.C. Reed: *Acta Mater.*, 2001, vol. 49, pp. 861–75.
15. Y. Wang, N.Q. Zhu, H. Wang, and X.G. Lu: *Metall. Mater. Trans. A*, 2017, vol. 48A, pp. 943–947.
16. T. Yamamoto, T. Takashima, and K. Nishida: *Trans. Jpn. Inst. Met.*, 1980, vol. 21, pp. 601–08.
17. G.C. Xu, Y.J. Liu, and Z.T. Kang: *J. Alloys Compd.*, 2017, vol. 709, pp. 272–76.
18. S.Y. Wen, Y. Tang, J. Zhong, L.J. Zhang, Y. Du, and F. Zheng: *J. Mater. Res.*, 2017, vol. 32, pp. 2188–2201.
19. M. Hattori, N. Goto, Y. Murata, T. Koyama, and M. Morinaga: *Mater. Trans.*, 2006, vol. 47, pp. 331–34.
20. J. Chen, and L.J. Zhang: *CALPHAD*, 2017, vol. 60, pp. 106–15.
21. J. Chen, L.J. Zhang, J. Zhong, W.M. Chen, and Y. Du: *J. Alloys Compd.*, 2016, vol. 688, pp. 320–28.
22. S. Hayashi, D.J. Sordelet, L.R. Walker, and B. Gleeson: *Mater. Trans.*, 2008, vol. 49, pp. 1550–57.
23. Q. Zeng, S.W. Ma, Y.R. Zheng, S.Z. Liu, and T. Zhai: *J. Alloys Compd.*, 2009, vol. 480, pp. 987–90.
24. E. Mabruri, M. Hattori, K. Hasuike, T. Kunieda, Y. Murata, and M. Morinaga: *Mater. Trans.*, 2006, vol. 47, pp. 1408–11.
25. W.M. Chen, L.J. Zhang, Y. Du, C.Y. Tang, and B.Y. Huang: *Scr. Mater.*, 2014, vols. 90–91, pp. 53–56.
26. W.M. Chen, J. Zhong, and L.J. Zhang: *MRS Commun.*, 2016, vol. 6, pp. 295–300.
27. HitDIC software: <https://hitdic.com/>. Accessed 21 December 2017.
28. J. Zhong, W. Chen, and L. Zhang: *CALPHAD*, 2017, vol. 60, pp. 177–90.
29. M.A. Dayananda: *Metall. Trans. A*, 1983, vol. 14A, pp. 1851–58.
30. W. Huang and Y.A. Chang: *Mater. Sci. Eng. A*, 1999, vol. 259, pp. 110–19.
31. L. Onsager: *Ann. N. Y. Acad. Sci.*, 1945, vol. 46, pp. 241–65.
32. J. L  chelle, S. Noyau, L. Aufore, A. Arredondo, and E. Audubert: *Diffus. Fundam. Org.*, 2012, vol. 17, pp. 1–39.
33. J.S. Kirkaldy, J.E. Lane, and G.R. Masson: *Can. J. Phys.*, 1963, vol. 41, pp. 2174–86.
34. J.S. Kirkaldy and D.J. Young: *Diffusion in the Condensed State*, Institute of Metals, London, 1987.
35. R.A. Swalin and A. Martin: *J. Metals*, 1956, vol. 8, pp. 567–72.
36. A. Volek, F. Pyczak, R.F. Singer, and H. Mughrabi: *Scr. Mater.*, 2005, vol. 52, pp. 141–45.
37. C.C. Jia, K. Ishida, and T. Nishizawa: *Metall. Mater. Trans. A*, 1994, vol. 25A, pp. 473–85.
38. T. Yokokawa, M. Osawa, K. Nishida, T. Kobayashi, Y. Koizumi, and H. Harada: *Scr. Mater.*, 2003, vol. 49, pp. 1041–46.